Spin-spin scattering in a silicon two-dimensional electron gas

Ruby N. Ghosh* and Robert H. Silsbee
Laboratory of Atomic and Solid State Physics, Cornell University, Ithaca, New York 14853-2051
(Received 6 April 1992)

The scattering of conduction electrons by neutral impurities in Si has been demonstrated through measurements of spin-dependent transport (SDT) in a two-dimensional electron gas (2DEG). SDT was observed by monitoring the conductivity of a specially fabricated Si accumulation layer transistor operating at 4 K while modulating the electron-spin populations. By utilizing the differences in the singlet and triplet state scattering cross sections, the technique provides the first *direct* measure of neutral impurity scattering. The SDT spectrum consists of a pair of hyperfine peaks separated by 42 G which are assigned to the impurity electron system and a broad central feature which is attributed to both the conduction spins and donor spins with strong exchange interactions. A phenomenological theory for the resonant change in device current is developed and comparison of theory with experiment indicates that the interaction of a 2DEG with neutral impurities must be treated two dimensionally; scaling the known 3D scattering cross sections to their 2D counterparts is inappropriate. Numerical simulations of the SDT line shape are obtained by modeling the spin dynamics. The possibility of alternative explanations for the observed signal, such as bolometric detection of the electron-spin resonance, are explored and eliminated. The SDT spectrum is characterized as a function of temperature, microwave power, Fermi energy of the 2DEG, and magnetic-field orientation. A lower bound for $\langle \Sigma_s - \Sigma_t \rangle$, the difference in singlet and triplet scattering cross sections integrated over angle and position of the donor impurity, is obtained as a function of the Fermi energy. A spin-dependent signal from $\sim 10^8$ spins was observed, which demonstrates the enhanced sensitivity of SDT over conventional electron-spin-resonance methods.

I. INTRODUCTION

The resistivity of a semiconductor at low temperature is expected to include a contribution from neutral impurity scattering. Within the effective-mass approximation, Pearson and Bardeen[1] noted in 1949 that the scattering of an electron off a neutral impurity was similar to the well-studied atomic physics problem of electron scattering by a hydrogen atom. In the low-energy limit, Erginsoy[2] obtained an expression for the relaxation time due to neutral impurity scattering τ_n which is independent of the velocity of the incident electron and scales with the density of neutral impurities. Further refinements were made by other authors and an extensive review of the various three-dimensional (3D) models of neutral impurity scattering can be found in Ridley.[3] Despite Pearson and Bardeen's suggestions in 1949, direct experimental measurements of neutral impurity scattering have been lacking to date. Indirect evidence has been obtained by two groups[4,5] by subtracting the calculated phonon and ionized impurity scattering rates from the measured Hall mobility.

Schmidt and Solomon[6] and Honig[7] independently proposed a direct demonstration of neutral impurity scattering by exploiting the difference in singlet and triplet cross sections for the scattering of conduction electrons from neutral impurities. The Pauli principle requires that the total wave function, which is a product of the spin and spatial components of the conduction electron–neutral impurity system, be antisymmetric with respect to the coordinates of the conduction and impurity electrons. Since the singlet and triplet spin wave function are antisymmetric and symmetric with respect to particle exchange, the difference between the two cross sections is due to the fact that the electrons will on average move in different regions of the potential in the different spin states, resulting in an effective spin dependence of the scattering potential. Application of a magnetic field to the sample polarizes the two spin species and increases the probability of finding the conduction and donor spins parallel, i.e., in the triplet state, during a scattering event. The spin-dependent scattering process then modifies the sample conductivity, which is detected as a change in the device current. We denote by spin-dependent transport (SDT) the dependence of conductance on spin polarization. SDT is observed by monitoring the device conductance while modulating the spin populations using standard electron-spin-resonance (ESR) techniques.

Maxwell and Honig[8] measured a spin-dependent photoconductivity signal at 4 K in Si samples doped with phosphorus (P) to 3.2×10^{16} cm^{-3} which was initially attributed to SDT. However, it was later shown[9] that the observed signal was due not to neutral impurity scattering but to the spin-polarization dependence of the electron trapping-recombination cycle. Electron-spin resonance of GaAs heterostructures[10] and other resonant processes has also been indirectly detected via bolometric response of the sample.[11]

In this paper we report on the first direct measurement of the scattering of spin $\frac{1}{2}$ conduction electrons off neutral impurities by detecting spin-dependent transport (SDT) in a Si two-dimensional electron gas (2DEG).[12] An

equilibrium population of conduction electrons is employed so that electron recombination is not an issue. SDT provides a high sensitivity indirect technique for observing ESR; our sample contains 10^8-10^9 spins, a number undetectable by conventional ESR methods. Section II describes the 4-K Si transistor specially fabricated for the experiment. Details of the modified ESR spectrometer used to observe SDT by monitoring the device current while modulating the electron-spin populations via standard techniques are also given. A formalism to describe the scattering of a 2DEG off neutral impurities is developed in Sec. III along with a discussion of the spin dynamics. Section IV presents the experimental evidence for spin-dependent transport and demonstrates that the bolometric sensitivity of our samples is far too low to be an operative mechanism. The dependence of the SDT signal on temperature, microwave power, Fermi energy of the 2DEG, and the magnetic-field orientation are explored in Sec. V. In Sec. VI we summarize our conclusions and discuss the potential for utilizing SDT as a probe of spin dynamics in confined semiconductor structures. A numerical simulation of the signal line shape is presented in the Appendix.

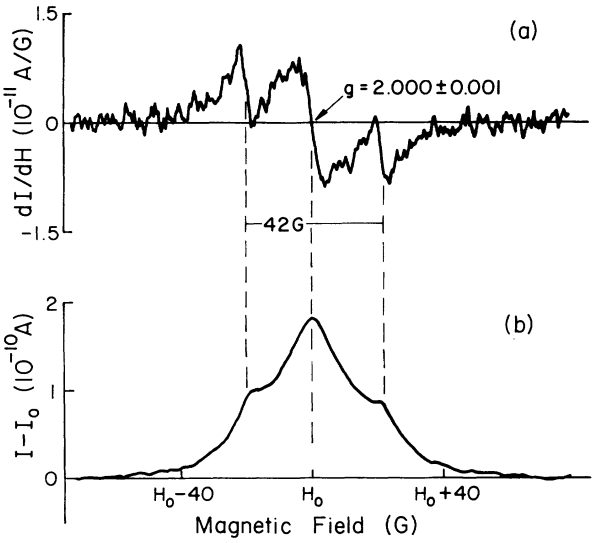

FIG. 1. (a) Derivative of the current and (b) the current itself as a function of magnetic field for sample 1; $n_s=0.57\times10^{12}$ cm^{-2}, $I_0=10.0$ μA, $H_0=3175$ G, microwave power $=4$ dBm, temperature $T=4.5$ K, and field modulation $H_{\rm mod}=2.5$ G$_{pp}$.

II. DEVICE FABRICATION AND MODIFIED ESR SPECTROMETER

The observation of spin-polarization effects in the conductivity of a Si sample presents several experimental challenges. The sample needs to be at low temperature to bind the impurity electron to the donor atom, thereby rendering it electrically neutral. As discussed previously, transport measurements must also be made without using photodegenerated carriers. These competing requirements were satisfied by fabricating a Si metal-oxide-semiconductor field effect transistor (FET), with an n-channel accumulation layer, that operates at 4 K. The degenerately doped source and drain contacts provide the equilibrium carriers for the 2DEG formed under the positively biased gate electrode. Therefore we have a variable density of free electrons scattering from a fixed number of neutral impurities. The substrate was a Si (100) wafer of thickness 0.41 mm doped with 2.7×10^{17} P/cm^3. The bulk doping density (N_D) was a compromise choice between two opposing criteria. To avoid effects due to impurity band conduction N_D needs to be below the metal-insulator transition which is 3×10^{18} cm^{-3} for Si:P. At the same time the neutral impurity scattering rate is proportional to the donor density[2] so N_D should be as large as possible to maximize the SDT signal. The diffusion of P impurities during the oxidation and annealing steps in the processing was carefully modeled and the calculated maximum P concentration at the oxide interface was 3.6×10^{17} donors cm^{-3}, still comfortably below the metal-insulator transition.

In order to observe spin-dependent transport by utilizing the difference between the singlet and triplet scattering cross sections, we modulate the electron-spin populations by driving the ESR transition. In the presence of dc and microwave fields when the Zeeman resonance condition is satisfied there will be a partial saturation of the spin polarization. Therefore in measuring the transistor current as a function of magnetic field, a resonant change $\Delta I/I_0$ is observed due to spin-dependent scattering (see Fig. 1). A half-wavelength microstrip resonator was incorporated into the transistor structure itself to modulate the spin polarization. For a free electron $g\sim2$ the Zeeman resonance condition will be satisfied at 9 GHz and 3200 G. The resonator consisted of a 1.00×5.28 (mm)^2 aluminum strip as discussed in Ref. 13.

The FET was fabricated in the middle of the microstrip resonator at a voltage node with the channel length perpendicular to the resonator strip.[13] The top metal film serves as both the upper conductor of the microstrip resonator and the gate of the FET. Placing the transistor in the middle of the resonator has two advantages: this is a position of maximum microwave magnetic field; and it is also a voltage node, so the conducting leads of the transistor are expected to minimally perturb the microwave fields of the resonant structure.

Details of the device and processing sequence have been previously described.[13,14] A compensating p implant was used to define a channel of length 1000 μm and width 100 μm via junction isolation. Four voltage probes were also included along the sides of the channel. The mobility was 3200 cm^2/V s, typical for a Si FET operating at 4 K. The SDT experiment was performed with the transistor operating in the linear region of its current-voltage characteristic to ensure a uniform 2DEG density (n_s) from source to drain. The 2DEG density ranged from 1.0×10^{11} cm^{-2} to 2.2×10^{12} cm^{-2} as determined via the Shubnikov-de Haas effect. These results agree with predictions from the device capacitance.

An x-band ESR spectrometer was modified to perform the SDT experiment. The Si sample was positioned inside a waveguide "stick" placed within a liquid He dewar. The FET current as a function of magnetic field, the SDT

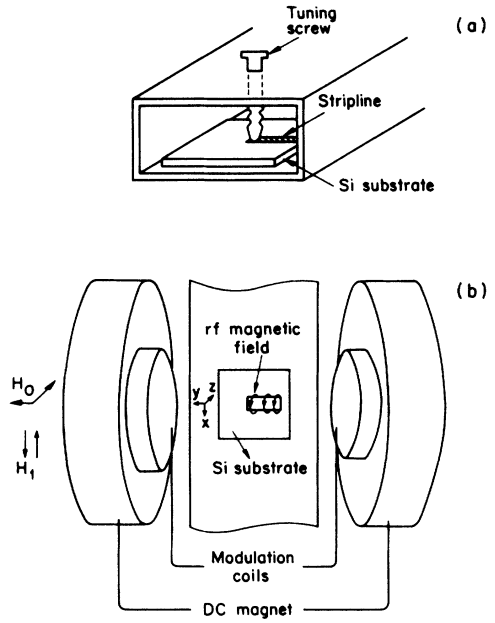

FIG. 2. (a) Schematic of the microwave coupling. (b) Orientation of the ac and dc magnetic fields with respect to the sample.

experiment, and the conventional ESR signal were measured. For the SDT experiment the spectrometer was used as a simple variable microwave power source. Figure 2(a) shows the scheme used to couple microwave power into the microstrip resonator. The coupler consisted of a tapered brass screw placed in the center of the wide face of the waveguide. The sample, with the strip length transverse to the guide, was positioned so that one end of the microstrip resonator was directly under the flat tip of the tuning screw. By varying the air gap between the tip of the screw and the microstrip resonator, the capacitive coupling could be adjusted.

For a spin-resonance experiment the rf magnetic field needs to be perpendicular to the dc magnetic field. The sample was mounted on the inside vertical face of the waveguide as shown in Fig. 2(b). The microwave magnetic-field lines circulate the stripline with $\mathbf{H}_1 = x H_1$ The dc magnetic field was rotated in the y-z plane as shown, where $\mathbf{H}_0 = \mathbf{y} H_0$ and $\mathbf{H}_0 = \mathbf{z} H_0$ correspond to having the field parallel and perpendicular to the semiconductor/oxide interface, respectively.

To measure the small change in device current due to the spin-dependent scattering a lock-in technique with magnetic-field modulation was used together with a low noise current amplifier. Using a 1-Hz bandwidth the current noise referenced to the input of the amplifier, varied from 5 to 50 pA/$\sqrt{\text{Hz}}$. A resonant change in device current $\Delta I / I_0$ as small as $\sim 5 \times 10^{-8}$ could be measured.

III. THEORY

In this section we develop a phenomenological theory for the resonant change in device current

$$\frac{\Delta I}{I_0} \equiv \frac{I - I_0}{I_0} \tag{1}$$

due to spin-dependent scattering. A first-principles derivation will ultimately require generalization of the theories of neutral impurity scattering (see review by Ridley[3]) from three to two dimensions. The off-resonance current I_0 is calculated from the device conductivity σ for the case of equilibrium spin polarization, while the on-resonance current I is obtained from the device conductivity for saturated spin polarization. We assume throughout that we are in the low-temperature limit, i.e., the Fermi energy (E_F) is much greater than kT, and that the velocity of the conduction electron is given by the Fermi velocity v. In subsection B of this section we discuss issues related to spin dynamics, and in subsection C the expected characteristics of the SDT signal based on our formalism.

A. Transport

The purpose of this work is to study the interaction between electrons and neutral donors, so we use an unconventional n-channel accumulation layer structure instead of a conventional n-channel inversion layer device. Note that paramagnetic resonance from acceptors in Si is difficult to observe in the absence of uniaxial stress.

The energy levels of n-type Si accumulation layers have been calculated by Ando[15] and Stern.[16] For an n-type substrate at low temperature, the Fermi energy in the bulk is pinned near the donor binding energy E_d, due to the residual concentration of acceptor impurities N_A. The negative space charge which neutralizes a positive gate bias applied to the gate is provided by the electrons trapped in the channel potential and by the ionized acceptor impurities N_A^-. The measured acceptor concentration in our wafers was $\sim 2 \times 10^{14}$ B/cm^3. The self-consistent potential and 2DEG density for a (100) Si surface with an acceptor concentration similar to our wafers ($N_A = 5 \times 10^{13}$ cm^{-3}) as calculated by Ando[17] are shown in Fig. 3. E_0, E_1, and E_2 are the minimum energies of the first three subbands derived from the Si conduction-band valleys with heavy mass direction perpendicular to the surface of the (100) sample. These results were obtained using the local-density-functional formalism and should contain effects of exchange and correlation. The 2DEG density in this experiment ranges from 1.0×10^{11} cm^{-2} to 2.2×10^{12} cm^{-2}, so single subband transport is expected.[15,17]

The scattering of an electron in the accumulation layer from an initial state $\Psi_i(\mathbf{r},z')$ to a final state $\Psi_f(\mathbf{r},z')$ is most easily treated within the framework of the Born approximation. Cylindrical coordinates are natural for this problem, and the z axis is in the direction perpendicular to the Si/oxide interface. We assume that the motion of the electron is free in the r-θ plane, and allow for the finite extent of the electron wave function in the z direction. Consider a neutral impurity located at $r = 0$ and at a distance z from the interface. The cross section for scattering of electrons from an initial to final state in two dimensions[18] by a scattering potential $\varphi(\mathbf{r},z';z)$ is

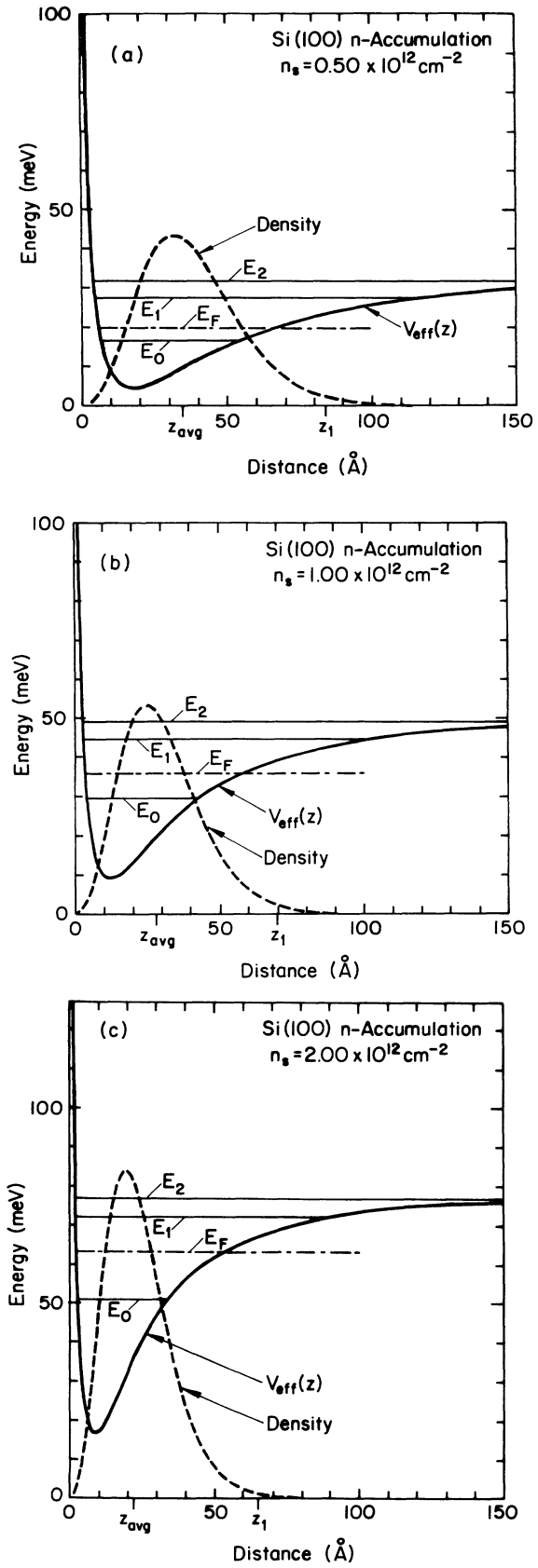

FIG. 3. Charge-density distribution of electrons, the self-consistent potential, and the edges of the subbands in an accumulation layer for several densities from Ando (Ref. 17).

$$\Sigma(\theta,z)=\frac{4\pi^2C^2m^*}{h^3v}|\langle\Psi_i|\varphi(\mathbf{r},z';z)|\Psi_f\rangle|^2\ , \tag{2}$$

where C is the area of normalization, m^* is the effective mass, h is Planck's constant, and v is the incident velocity of the electron. From the above equation and Fig. 3 it is clear that the spatial extent of the electron wave function, which is a function of the 2DEG density (n_s), contributes to the z dependence of the neutral impurity scattering cross section. This is particularly true for the z's of interest to us which turn out to lie in the weak tails of the electron charge density. The average distance of the electrons from the interface varies from 40 to 20 Å as n_s increases.

The range of the effective scattering potential φ also depends on the distance of the impurity from the interface. A reasonable estimate of that range is the radius of the outer electron in a negative hydrogenic ion H^-. Chandrasekhar's[19] wave function for H^- gives a value of $2.1a_0$ (a_0 is the Bohr radius) for the radius of the "second electron." Within the framework of the effective-mass approximation and using both the measured and calculated hydrogenic binding energies for bulk Si:P, we obtain a radial range of 20–40 Å. However, the binding energy of an impurity located near the semiconductor/oxide interface is a function of the donor distance from the interface,[20] due to the spatial variation of the electric field in that region (see Fig. 3). Therefore the range of the effective scattering potential for neutral impurities located within the penetration depth of the 2DEG will be a function of z.

Critical to our discussion is the cutoff in the distribution of neutral impurities due to the band bending at the semiconductor/oxide interface. A neutral P donor impurity can capture a second electron to form a doubly occupied P^- ion which has a binding energy of 3.7 meV for bulk Si:P.[21] The effect of the P^- state is that only those donors in the region where $E_c-E_f>4$ meV are neutral, the remaining donors near the interface are doubly occupied and do not contribute to the SDT signal. The boundary between singly/doubly occupied donors is defined as z_1, and $65\le z_1\le 85$ Å as shown in Fig. 3. We note that this definition of z_1 is only a first approximation for it does not account for the spatial dependence of the P^- binding energy noted in the preceding paragraph.

Let $N(z)$ be the volume density of neutral impurities, which is given by

$$\begin{aligned} N(z)&=0 \quad z<z_1 \\ &=N_D \quad z\ge z_1\ . \end{aligned} \tag{3}$$

Summing the contribution from each scatterer acting independently, the momentum scattering rate due to neutral impurities is

$$\frac{1}{\tau_n}=N_D\int_0^{2\pi}d\theta(1-\cos\theta)\int_{z_1}^{\infty}dz\,v\Sigma_n(\theta,z)\ , \tag{4}$$

where Σ_n is the neutral impurity scattering cross section, suitably averaged over the singlet and triplet channels, and v is the velocity of the incident electron.

Application of a magnetic field will polarize the con-

duction and impurity electron spin systems. From simple quantum mechanics Σ_n can be written in terms of the spin polarizations and the singlet and triplet cross sections Σ_s and Σ_t as[6,7]

$$\Sigma_n = \Sigma_0[1-\beta P_i P_c] , \tag{5}$$

where

$$\Sigma_0 \equiv (\Sigma_s + 3\Sigma_t)/4, \quad \beta \equiv (\Sigma_s - \Sigma_t)/(\Sigma_s + 3\Sigma_t) .$$

P_i and P_c are the impurity and conduction electron spin polarizations respectively. The crux of the SDT technique is to exploit the *difference* between the singlet and triplet scattering cross sections contained in the parameter β, to measure spin-dependent processes. Unfortunately, we are not aware of any 2D calculations of Σ_s and Σ_t, so they must remain free parameters in our formalism.

To measure spin-dependent processes the sample is irradiated with a fixed microwave power level and the transistor current is monitored as a function of dc magnetic field. We account for the degree to which the microwave field destroys the spin polarization by introducing the impurity and conduction spin saturation parameters s_i and s_c, respectively, as

$$\begin{aligned} P_i &\equiv P_i^0(1-s_i) , \\ P_c &\equiv P_c^0(1-s_c) , \end{aligned} \tag{6}$$

where P^0 is the equilibrium or off-resonance polarization. s_i or s_c have simple physical interpretations: they represent the ratio of the microwave power absorbed by the particular spin system to the maximum power that can be absorbed.[13] s ranges from zero to one, with $s=1$ corresponding to complete saturation. A more detailed discussion of the saturation parameters are contained in the section on spin dynamics.

The equilibrium spin polarizations are obtained as follows. The impurity electrons are treated as a classical gas which obeys Boltzmann statistics. At a given temperature T and magnetic field H_0, P_i^0 is

$$P_i^0 \approx \left[\frac{g\mu_B H_0}{2kT} \right] , \tag{7}$$

where g is the Landé g factor, μ_B the Bohr magneton, k the Boltzmann constant. The approximation is valid for the range of magnetic fields and temperatures employed in our experiment, $H_0 \sim 3200$ G and $2 \le T \le 5$ K. The conduction electrons are a two-dimensional degenerate Fermi gas; thus their equilibrium polarization is

$$P_c^0 = \frac{g\mu_B H_0}{2(E_f - E_0)} , \tag{8}$$

where E_0 is the bottom of the first subband (see Fig. 3). An important difference between the two systems is that the impurity electron polarization varies inversely with temperature, while the conduction electron polarization is independent of temperature.

The neutral impurity scattering rate in the presence of magnetic resonance can be written as

$$\begin{aligned} &\frac{1}{\tau_n} = \frac{1}{\tau_{n0}}[1-\alpha P_i^0 P_c^0 (1-s_i)(1-s_c)] , \\ &\frac{1}{\tau_{n0}} \equiv \frac{N_D v}{4} \langle \Sigma_s + 3\Sigma_t \rangle \quad \text{and} \quad \alpha \equiv \frac{\langle \Sigma_s - \Sigma_t \rangle}{\langle \Sigma_s + 3\Sigma_t \rangle} \end{aligned} \tag{9}$$

by using Eq. (5) in Eqs. (4) and (3). The angular brackets represent a suitable integral over θ and z as appropriate in calculating a momentum scattering rate. In two dimensions the angular brackets are given by

$$\langle F \rangle \equiv \int_0^{2\pi} d\theta (1-\cos\theta) \int_{z_1}^{\infty} dz\, F(\theta, z) . \tag{10}$$

The formula for $1/\tau_n$ could also be used in 3D, for the dimensionality of the problem is contained in the definition of $\langle F \rangle$. In writing Eq. (9) we have assumed that the parameters s_c and s_i are independent of the position of the neutral impurity. Since $1/\tau_{n0}$ is the neutral impurity scattering rate for zero polarization, Eq. (9) illustrates how the difference in the singlet and triplet scattering cross sections (contained in α), the equilibrium spin polarization, and the rf field work to change that scattering rate on resonance.

In order to calculate the change in device current on-resonance we need to account for all the scattering processes that contribute to the conductivity, σ. At 4 K these will be surface roughness scattering, scattering due to charged centers in the oxide, and neutral impurity scattering. Using Matthiessen's rule, the total scattering rate $1/\tau_t$ can be expressed as

$$\frac{1}{\tau_t} = \frac{1}{\tau_0} + \frac{1}{\tau_n} , \tag{11}$$

where $1/\tau_0$ is the scattering rate due to all other processes beside neutral impurity scattering. $1/\tau_t$ is known from the measured transistor mobility. The neutral impurity scattering rate off-resonance is given by letting $s_i = s_c = 0$ in Eq. (9). Letting I and I_0 be the current on- and off-resonance, respectively, the change in current due to spin-dependent transport is calculated from the conductivity using Eq. (11) and Eq. (9) as

$$\begin{aligned} \frac{\Delta I}{I_0} &\equiv \frac{I - I_0}{I_0} \\ &= \frac{\sigma}{\sigma_0} - 1 \\ &= \frac{1 + \tau_0/\tau_{n0}[1-\alpha P_i^0 P_c^0]}{1 + \tau_0/\tau_{n0}[1-\alpha P_i^0 P_c^0 (1-s_i)(1-s_c)]} - 1 . \end{aligned} \tag{12}$$

We justify linearization of this equation by showing that the second term in the square brackets in the denominator is much less than one. Letting $g \sim 2$, the equilibrium impurity polarization at 4 K from Eq. (7) is $P_i^0 = 0.051$. Similarly from Eq. (8), the conduction electron polarization over the range of 2DEG densities used in the experiment is $0.0012 \le P_c^0 \le 0.029$. By definition $0 \le \alpha \le 1$ and $0 \le [(1-s_i) \text{ and } (1-s_c)] \le 1$. Keeping only first-order terms in Eq. (12) we have

$$\frac{\Delta I}{I_0} \cong -\alpha P_i^0 P_c^0 s \frac{1/\tau_n}{1/\tau_t} ,$$

$$\text{where } s \equiv [1-(1-s_i)(1-s_c)] . \quad (13)$$

Equation (13) is the principal result of this section. The change in device current due to spin-dependent transport is proportional to the difference between the singlet and triplet scattering cross sections (via α), the product of the equilibrium polarizations of the two spin systems, and a saturation parameter, all weighted by the relative strength of the neutral impurity to total scattering rates. The sign of $\Delta I/I_0$ is determined by the relative strengths of Σ_s and Σ_t. In 3D the scattering cross sections are functions of energy[22] and the sign of α is found to vary with energy; similar behavior is anticipated in the present 2D case. In order to maximize the strength of the SDT signal, the scattering due to all other mechanisms should be comparable with the neutral impurity scattering rate.

The above definition of the saturation parameter s indicates that at high microwave power full saturation of either the conduction or impurity spins or both spin populations together results in a constant SDT signal independent of power. Note that this behavior is unlike a homogeneously broadened ESR line which decreases with increasing power above saturation. An important difference between the SDT and ESR experiments is that the SDT signal is proportional to the normalized spin polarization or fractional difference between the populations of the spin-down and spin-up states $(n_+ - n_-)/(n_+ + n_-)$, while the ESR signal depends on the magnetization and hence varies directly as the population difference $(n_+ - n_-)$.

B. Spin dynamics

The theory presented in Sec. III A predicts the magnitude of the SDT signal in terms of the saturation parameters s_i and s_c. We describe here the ingredients of a theory of the spin dynamics for a model system which predicts several important features of the shape of the resonance-induced saturation. The task is to determine the saturation parameters entering Eq. (13) under specified conditions of magnetic field, frequency, and microwave power. We model the spin dynamics by a set of coupled Bloch equations, one for the conduction electrons, and a large set of equations for the impurities in successive planes at increasing depth z. For each layer of impurity spins we write two Bloch equations, one to describe the impurities with donor nucleus with spin-up, the other for donors with nuclei with spin-down. We suppose any nuclear-spin-flip rate to be too small to influence the dynamics of interest in the SDT. The Bloch equations for the impurities include a term reflecting exchange scattering with the conduction electrons with a rate constant $1/T_{ix}(z)$. Since impurities for $z < z_1$ are doubly occupied and not paramagnetic, our interest is only in impurities at depths $z > z_1$. For these, the exchange rate decreases rapidly with decreasing depth z. Lengths relevant to this issue include the attenuation length for the tail of the charge density of the channel electrons (see Fig. 3) and the orbit radius of the donor states.

In addition to the exchange coupling of the impurity spins to the conduction spins, there is direct coupling among the impurity spins as described in Refs. 23 and 24. This coupling strongly influences the line shape but is omitted from the simplified model, which therefore may be used to gain useful insights but not for quantitative comparisons with experiment.

We distinguish among three groups of neutral impurity spins. By strongly coupled impurities we denote those whose exchange rate with the conduction spins is faster than the hyperfine coupling. These spins play two distinct roles in the generation of the SDT signal. First they absorb power from the microwave field, reducing their polarization $P_i = (1-s_i)P_i^0$, and reducing as well that of the conduction electrons via the exchange scattering. Second, these are the spins whose polarization determines the spin dependent conductance; because of the exponential decrease of electron density with depth, the only significant contribution to the intregrated cross section defined by Eq. (10) is from those impurities within a few tens of Å of z_1. Weakly coupled impurities are defined as those for which the exchange rate is intermediate between the hyperfine coupling and a slower cutoff relaxation rate $1/T_{i0}$, the bottlenecked spin-lattice relaxation rate for the full coupled spin system. These contribute, through resonant absorption of microwave power, to the saturation of the spin polarizations of themselves and, via the $1/T_{ix}$ process, of the conduction spins and of the strongly coupled spins. Note, however, that these spins do not directly influence the conductance because of the weakness of their exchange coupling. Finally come the uncoupled impurities, those for which the exchange scattering is weak compared with the cutoff relaxation rate. These may have saturated polarization, but are irrelevant to the SDT because they neither scatter strongly enough to contribute any spin dependence to the conductance nor do they couple strongly enough to the rest of the spin system to contribute to its saturation.

The anticipated line shape of the SDT signal consists of several components. First is a central contribution at $g \sim 2.00$ (Ref. 25) from the conduction electrons, with a width containing contributions both from the conduction electron transverse relaxation time T_{c2} and from the exchange coupling with the impurity spins. Next is a contribution from donors far from the conducting channel, the weakly coupled spins. For these the spin dynamics will be as described in Refs. 23 and 24, in which the authors derive a complex spectral shape with a pair of hyperfine split lines (full splitting of 42 G), from donors well isolated from other donors, and a complex structure between these lines, contributed by exchange coupled pairs, triples, and clusters of donors for which the direct exchange is strong enough to give exchange narrowing of the hyperfine interactions. For our problem, the weak exchange coupling with the conduction electrons gives some additional broadening to this structure but is not a major perturbation. The contribution of the weakly coupled impurity spins to the SDT line shape is expected to

be essentially the shape discussed in Refs. 23 and 24. However, for the strongly coupled donors close to the channel, the exchange scattering of the conduction electrons against the donors gives narrowing of the hyperfine splitting for all donors without regard to the degree of clustering. Hence these donors contribute only to the density of the line centered at $g \sim 2.00$, and with a width which decreases with increased strength of the exchange scattering $1/T_{ix}$ relative to the hyperfine splitting.

In order to estimate s_i we note that the integral of Eq. (4) is completely dominated, through $\Sigma_n(\theta,z)$, by the strongly coupled impurities near z_1 because of the rapid attenuation of the conduction electron wave function with increasing depth. However, these impurities are so strongly coupled to the conduction electron via the exchange scattering that they will have a spin temperature and saturation parameter which are the same as those of the conduction electrons. Thus, for those impurities whose spin polarization contributes to the change in channel conductance, the saturation parameter s_i may be set equal to the s_c of the conduction electrons. Those impurities at larger z, both weakly coupled and uncoupled, will be more heavily saturated but their degree of saturation is irrelevant since they make negligible contributions to the integral of Eq. (4).

In calculating the saturation parameter s_c, however, it is essential to treat both the strongly and the weakly coupled spins; the relaxation of both to the lattice is ultimately through the conduction electrons. The saturation parameters $s_i = s_c$ are finally determined by a balance in steady state between microwave power being absorbed by all three species, the conduction electrons and both the strongly and weakly coupled impurities, and energy transfer from the conduction spins to the lattice by the conduction electron relaxation $1/T_{c1}$. It is straightforward to calculate the power absorbed in the limit of weak saturation and the argument in the Appendix is restricted to this limit. The assumption both obviates the need to work out the z dependence of the saturation parameter and allows linearization of the Bloch equations.

Because we are unable to include the effects of the cluster exchange in the coupled set of Bloch equation which we use to model the dynamics of this system, the model, though useful in giving insight into the essential physics, does not give results which may be compared with the experimental data. Model calculations and conclusions from them are described in the Appendix.

C. Summary

A quantitative comparison of our experimental results with the formalism developed to describe the scattering of a 2DEG off neutral impurities [Eq. (13)] requires knowledge of the appropriate cross sections. Since the singlet and triplet scattering cross sections have been calculated in 3D,[22] it is tempting to scale the known 3D results to their 2D counterparts by dividing by an appropriate length. In Sec. III A we estimated that the range of the effective scattering potential was 20–40 Å, the average spatial extent of the 2DEG was 20–40 Å, and z_1, the distance beyond which the donor impurities were neutral, was 65–85 Å. The comparable magnitude of these three length scales indicates that a simple but meaningful conversion of the 3D cross sections to 2D cross sections is not possible. In addition the 3D cross sections are functions of energy so it is necessary to calculate the corresponding 2D donor binding energy to scale the energy dependence. However, the 2D binding energy of the neutral impurities ($z \geq z_1$) will be a function of z because of the position-dependent electric field within the semiconductor. A z-dependent binding energy further complicates a construction of a reasonable method to scale from three to two dimensions.

We can experimentally verify the inadequacy of using the 3D cross sections for this experiment. In the limit where the wave vector k is zero, $\Sigma_s > \Sigma_t$ in 3D (Ref. 22) so Eq. (9) indicates that $\alpha > 0$. From the expression for the SDT current on-resonance equation (13), the 3D results predict that $\Delta I/I_0 < 0$ at low energy. This prediction will be shown to be contrary to our experimental results in Sec. V B. Therefore only a 2D calculation of the scattering cross section will allow for a proper comparison of theory with experiment.

The SDT measurement is performed with the transistor operating in the linear region of its current-voltage (I-V) characteristic, where the 2DEG density is constant from drain to source. Since the SDT signal is due to a polarization-induced change in the conductivity, $\Delta I/I_0$ at a fixed gate bias is expected to be a constant independent of I_0. As discussed in Sec. IV, this feature of the SDT spectra together with other measurements to help distinguish the spin-dependent scattering mechanism from other resonant processes such as ESR-induced heating of the 2DEG.

IV. EXPERIMENTAL EVIDENCE FOR SPIN-DEPENDENT TRANSPORT

A. Overview of data

An overview of the SDT data is presented in this section Extensive measurements on two different devices, sample 1 and sample 2, were performed; most of the data in this section are from sample 1. The 2DEG density ranges from 1.0×10^{11} cm^{-2} to 2.2×10^{12} cm^{-2} in our experiment. Unless otherwise indicated the dc magnetic field is oriented parallel to the plane of the 2DEG, $\mathbf{H}_0 = \mathbf{y}H_0$ as shown in Fig. 2(b).

A lock-in technique was used to measure the small change in current due to spin-dependent scattering. Figure 1 shows a typical pair of derivative and integrated spectra at $n_s = 0.57\times10^{12}$ cm^{-2}. The observed line shape has a broad central feature with a g value of 2.000 ± 0.001 and two narrow features displaced almost symmetrically by 21 G to either side of the center. The split components are attributed to the impurity electron spins. The impurity electrons are bound to phosphorus (P) donor nuclei that have a nuclear spin of $\frac{1}{2}$. From ESR experiments on bulk Si:P, it is well known[25] that the hyperfine interaction between the localized impurity electron and donor nucleus splits the observed resonance by 42 G. Therefore we assign the two narrow peaks to the

impurity electron-spin system. As noted in Sec. III B, we also expect a central feature with contributions from three sources: the conduction electron spins, exchange narrowed clusters of weakly coupled donor impurities and impurity spins that are strongly coupled to the conduction spins via $1/T_{ix}$ processes. The line shape will be discussed in greater detail in Sec. V. Our g value agrees, within experimental error, with previous measurements of the g value of conduction electrons in Si.[25]

The observed change in current on-resonance in our experiment is due to a change in the device conductance resulting from spin-dependent scattering processes. For a fixed gate voltage the SDT signal $\Delta I/I_0$ is expected to be independent of I_0. Measurements were made on both samples at several points on the current-voltage (I-V) characteristic, below saturation, over the full range of gate biases. $\Delta I/I_0$ was found to be approximately constant, indicating that the SDT signal is independent of the source-drain electric field as expected for a spin-polarization-induced conductivity change.

The lock-in technique significantly improves the signal-to-noise ratio but determination of the sign of the signal requires careful accounting for all the phase changes induced by the measurement circuit. Instead, the sign of the signal was determined very directly by making a dc measurement of the current while sweeping the magnetic field. Identical values for the magnitude of the SDT signal were obtained from the dc measurement and integration of the simultaneous ac or lock-in data. By keeping careful track of the lock-in phase settings relative to the settings for this run, the signs of all the ac measurements were referenced to this dc measurement.

Using the expression for the SDT current on-resonance equation (13) we calculate a lower bound on the difference between the singlet and triplet scattering cross sections $\langle \Sigma_s - \Sigma_t \rangle$ from our data. If we assume that the SDT signal is fully saturated, i.e., $s=1$, then $\Delta I/I_0$ can be written as

$$\frac{\Delta I}{I_0} = -P_i^0 P_c^0 \frac{\tau_t N_D v}{4} \langle \Sigma_s - \Sigma_t \rangle , \tag{14}$$

using Eq. (9) in Eq. (13). The measured device mobility of 3200 $\mathrm{cm^2/V\,s}$ gives a total scattering rate of $1/\tau_t = 2.9\times10^{12}\ \mathrm{s^{-1}}$ and $P_i^0=0.05$ and $P_c^0=0.005$ for the experimental conditions in Fig. 1. From the peak SDT signal of $\Delta I/I_0 = 2\times10^{-5}$ we obtain a lower bound for the difference in integrated singlet and triplet scattering cross section of $\langle \Sigma_s - \Sigma_t \rangle \geq 4\times10^{-13}\ \mathrm{cm^2}$ at a density of the 2DEG of $n_s = 0.57\times10^{12}\ \mathrm{cm^{-2}}$. The angular brackets represent the integral over θ and z as defined in Eq. (10). We may estimate a value for the 2D SDT cross section difference ($\Delta\Sigma_{\mathrm{SDT}}$) by dividing $\langle \Sigma_s - \Sigma_t \rangle$ by the range of the scattering potential (z^*),

$$\langle \Sigma_s - \Sigma_t \rangle \equiv \Delta\Sigma_{\mathrm{SDT}} \times z^* . \tag{15}$$

In the Appendix we estimate z^* to be 60 Å, which gives $\Delta\Sigma_{\mathrm{SDT}} \geq 70$ Å for the difference of the 2D scattering cross sections. This is a reasonable result since $\Delta\Sigma_{\mathrm{SDT}}$ is of the same order of magnitude as the other three length scales (z_{avg}, z_1, and z^*) in our formalism.

To check for spurious effects associated with microwave rectification in the contacts, the four probe measurement shown in Fig. 4 was performed. The upper traces shows the normalized current signal using our standard two probe (source-drain) setup. The lower trace is the normalized voltage signal measured via a four probe method. The fractional SDT signal is identical in both cases, ruling out effects due to rectification in the contacts. In addition we note that the n^+ contacts were doped with arsenic (As) which has a nuclear spin of $\frac{3}{2}$. A spin-resonance signal from the contacts would have either a single exchange narrowed line or four hyperfine split peaks, in contradiction to the observed spectra.

We briefly consider another mechanism, based on the energy dependence of the mobility, which could result in a spin dependence of the device conductivity and show that it is not applicable to our experiment. When the electron system is spin polarized there are different numbers of electrons in the spin-up and spin-down states, so any energy-dependent scattering mechanism would then result in a change in the sample conductance (σ). The fractional change in conductance when the spin populations are fully equalized by spin-resonance saturation, compared with the spin-polarized equilibrium state, is given by

$$\frac{\Delta\sigma}{\sigma} = -\frac{1}{\mu}\left[\frac{g\beta H}{2}\right]^2 \left[\frac{1}{E_f}\left[\frac{d\mu}{dE}\right] + \frac{1}{2}\left[\frac{d^2\mu}{dE^2}\right]\right] , \tag{16}$$

where μ is the energy-dependent mobility of the electrons. The magnitude of this contribution may be evaluated from experimental data on the dependence of mobility on Fermi energy.[13] Over most of the experimental range of E_F, the predicted signal is an order of magnitude or more smaller than the observed signal and it changes sign in the middle of the range of concentrations measured (the mobility goes through a maximum in this

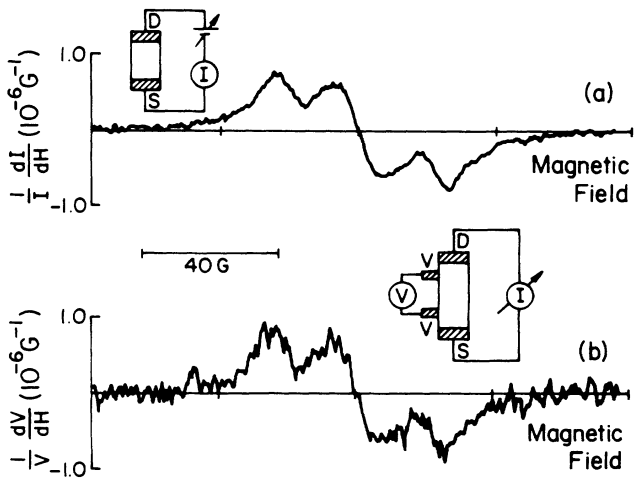

FIG. 4. (a) Normalized current signal as measured via the two probe setup. (b) Normalized voltage signal as measured via the four probe setup. Both traces are from sample 1, $n_s = 0.57\times10^{12}\ \mathrm{cm^{-2}}$, microwave power is equal to 10 dBm, and $H_{\mathrm{mod}} = 10\ \mathrm{G}_{pp}$.

range), in clear disagreement with the data to be presented in Fig. 10.

B. Bolometric detection of ESR

Another possible source of the observed signal is bolometric detection of ESR in the sample. By bolometer we mean a temperature sensor or a device whose output signal depends on the temperature of the device. Several investigators[11,26] have measured and modeled the effect of the 2DEG temperature (T_e) on the conductivity of a Si metal-oxide-semiconductor field-effect transistor (MOSFET). Stein, Klitzing, and Weimann reported the first indirect ESR measurements of a 2DEG by observing the ESR-induced change in magnetoresistivity of an $Al_xGa_{1-x}As/GaAs$ structure due to electron heating. The proposed bolometric mechanism would then be absorption of electromagnetic energy on resonance by the impurity or conduction spins, which would modify T_e and be detected as a change in the transistor current. We exploit the idea that the bolometric response of the FET $d\sigma/dT_e$ must be independent of the mechanism by which the electron temperature is altered to predict magnitudes of two possible bolometric mechanisms. We consider detection both of the bulk ESR (Mechanism 1) and of the channel ESR (Mechanism 2), and show that neither can be responsible for the current signal attributed to SDT.

Once the FET is mounted into the spectrometer both the conventional ESR signal and the current can be measured. Figure 5(d) shows the standard ESR absorption spectrum of sample 1, taken at zero gate bias. The line shape is as expected[23] for bulk Si doped to 3×10^{17} P/cm^3, donor clusters contributing to the structure between the hyperfine lines. The power dependence of the central and hyperfine components suggests an inhomogeneously broadened line with the unity saturation point at about -15 dBm.

Figure 6 shows the bolometric response of sample 2 in the absence of magnetic resonance. I^0 is the transistor current at the lowest measured level of microwave power. At low microwave power (P_μ) the FET current has a positive but saturating nonlinear dependence on P_μ, which we interpret as a change in channel conductance produced by heating of the sample via microwave dissipation in the microstrip resonator. At higher powers, the slope of $d(I-I^0)/dP_\mu$ decreases then changes sign above 10 dBm. Similar results were obtained from Sample 1.

The current spectrum of the transistor was measured over four and a half decades of power from 13 to -35 dBm at both 4.2 and 2.3 K. The low-temperature data will be discussed in the next section. Representative current spectra are shown in the upper portion of Fig. 5, along with the conventional ESR spectrum in the lower portion of the figure. The high power signal (a) which we attribute to SDT has a different line shape than the ESR signal (d). As the power is decreased there appears a fascinating *new signal* of the opposite sign and a *different line shape.* Note that the line shape of spectrum (c) is similar to the ESR line shape (d), but different from the SDT signal (a). We show below that the low power signal (≤ -20 dBm) is due to bolometric detection of the bulk phosphorus donor ESR via mechanism 1.

Figures 7(a)–7(b) give a schematic representation of our model for mechanism 1. Off resonance the incident microwave power ($P_{\rm inc}$) is partially reflected ($P_{\rm refl}$) and the rest is absorbed by the stripline ($P_{\rm strip}$). $P_{\rm strip}$ then heats the 2DEG, giving rise to the bolometric response $I-I^0$ shown in Fig. 6. On resonance, microwave power is absorbed by both the ESR of the bulk spins ($P_{\rm ESR}$) and the stripline. The bulk impurity spins transfer their excess energy to the Si lattice via spin-lattice relaxation processes $1/T_{i1}$. For an undercoupled cavity, the extra losses induced by a paramagnetic sample degrades the

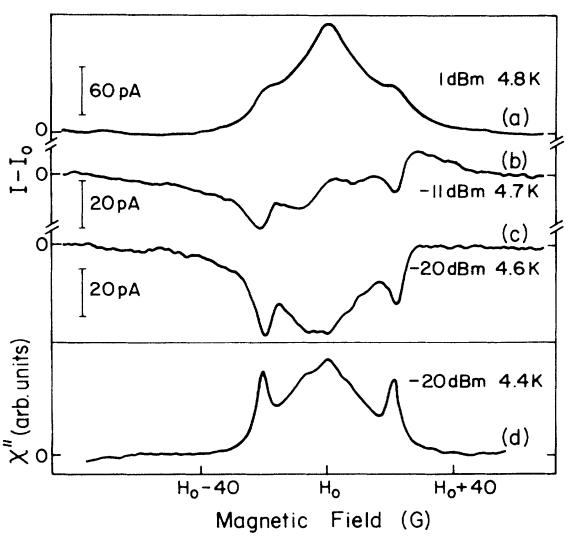

FIG. 5. (a)–(c) Current as a function of magnetic field for various microwave power levels from sample 1; $n_s=0.57\times10^{12}$ cm^{-2}, $I_0=10.0$ μA, and $H_{\rm mod}=5$ G_{pp}. (d) Absorption ESR spectrum from sample 1; $H_{\rm mod}=1.2$ G_{pp}.

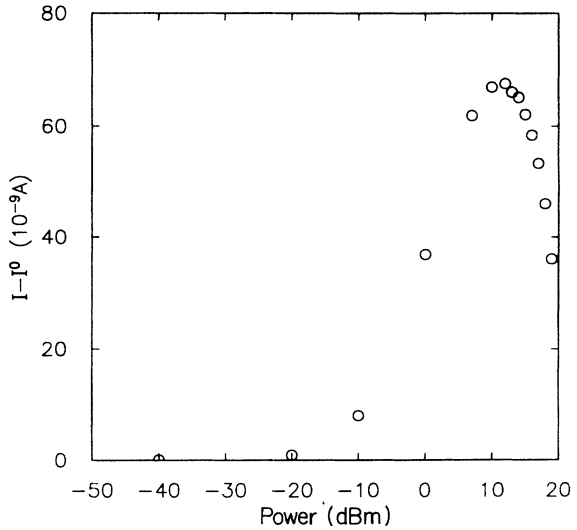

FIG. 6. Bolometric response curve for sample 2 in the absence of magnetic resonance; $n_s=0.57\times10^{12}$ cm^{-2}, $I^0=20.05$ μA (at -100 dBm), and $T=4.3$ K (at -100 at dBm).

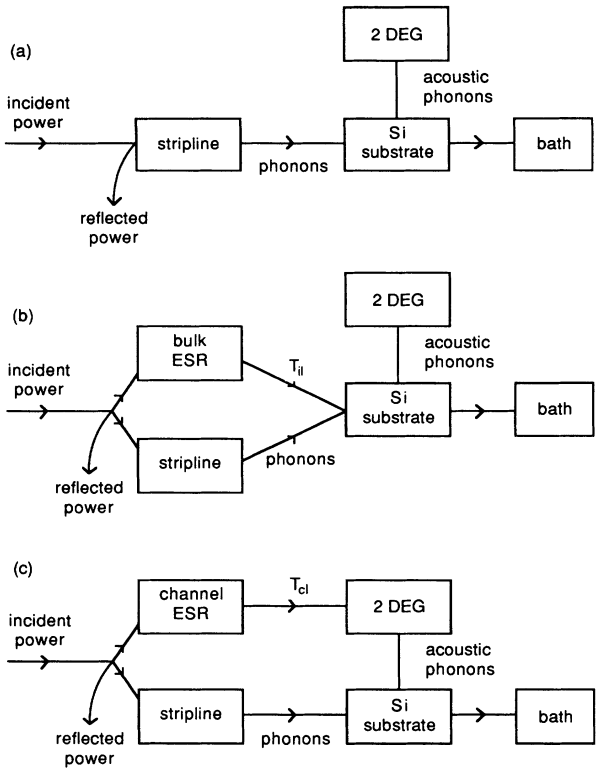

FIG. 7. Schematic of the bolometric response of the FET (a) off-resonance, (b) Mechanism 1 on-resonance, and (c) Mechanism 2 on-resonance.

coupling on-resonance to give an increase in reflected power and a decrease in the net power absorbed ($P_{\text{strip}}+P_{\text{ESR}}$) by the sample. Consequently there is a *decrease* in the heating of the 2DEG on-resonance. In Fig. 5(c) the transistor current decreases when the dc magnetic field satisfies the bulk spin resonance, tracing out a line shape similar to that observed for conventional ESR of the bulk [Fig. 5(d)].

The magnitude of the observed low power current signal at -20 dBm and 4.6 K for Sample 1 [Fig. 5(c)] is consistent with the calculated ESR dissipation together with the bolometric sensitivity determined from $I(P_\mu)$ characteristic. The bolometrically detected ESR line is assumed to be unsaturated since the conventional ESR spectra does not saturate until about -15 dBm. The number of bulk phosphorus donors within the volume of the microstrip resonator is 6×10^{14} spins. We estimate the loaded Q to be about 100 and use the full width at half maximum of the central feature in Fig. 5(c) to obtain T_2, the spin-spin relaxation time. The power absorbed by the bulk spins is then calculated to be $P=1.0\times10^{-7}$ W. Using a bolometric sensitivity of 4×10^{-4} A/W obtained from the slope of the $I(P_\mu)$ characteristic at -20 dBm, we estimate the bolometrically detected signal to be ~40 pA, in agreement with the measured value of 40 pA. We attribute the low power current signal (≤-20 dBm) to bolometric detection of the bulk phosphorus ESR by an undercoupled cavity based on the sign, line shape, and estimated magnitude of the signal.

Similar arguments rule out the possibility that the high power SDT signal (≥-8 dBm) is due to Mechanism 1 for the following two reasons. The line shape is not the same as the bulk ESR [compare Fig. 5(a) with 5(c) or 5(d)]. Second, since the measured bolometric response for the sample is positive below 10 dBm,[13] the sign of the high power current signal is inconsistent with bolometric detection of the bulk ESR [compare Fig. 5(a) with 5(c)].

A second bolometric mechanism we need to consider, Mechanism 2 shown in Fig. 7(c), is the direct heating of the 2DEG via the ESR of the channel. By ESR of the channel we are referring to both the conduction electrons and the impurity electrons located within the penetration depth of the 2DEG wave function, which we estimate from Fig. 3 to be 100 Å. In order to observe the impurity electron resonance via this mechanism the impurity-conduction mutual spin-flip rate $1/T_{ix}$ would have to be fast compared to $1/T_{i1}$. On-resonance the spin degrees of freedom of the 2DEG would absorb microwave power which would then be transferred to the kinetic degrees of freedom of the 2DEG via $1/T_{c1}$ processes to give an electron kinetic temperature higher than the lattice temperature. The high power SDT signal [Fig 5(a)] will be shown not to be due to Mechanism 2 in the remainder of this section.

We now compare the high power current signal at 1 dBm and 4.2 K [see Fig. 5(a)] with an upper bound for the bolometrically detected ESR signal from the channel impurity electrons. Within the 1000×100 $(\mu\text{m})^2$ channel region there are $\sim3\times10^8$ impurity spins. Assuming an unsaturated line and using the full width at half maximum of the central feature in Fig. 5(a) for T_2 we find that the power absorbed by the channel impurity electrons[13] is $P=16$ pW. At first glance it appears that the channel ESR signal would be impossibly small to detect because there are 10^6 fewer spins in the channel than the bulk. However, since the channel ESR dissipates its power directly into the 2DEG we must account for the thermal impedance between the 2DEG and the lattice in calculating the bolometric sensitivity.

The dissipation of the excess electronic thermal energy is limited by electron-acoustic phonon scattering processes τ_{ep}.[13] Letting C_e be the electronic specific heat appropriate for a degenerate 2DEG, the thermal impedance between the 2DEG and lattice R_{ep} obtained from the energy balance is

$$R_{\text{2DEG}-I}=\frac{\tau_{\text{ac}}}{C_e}=\tau_{\text{ac}}\frac{3h^2}{8\pi^3k^2Tam^*}\,, \tag{17}$$

where h is Planck's constant and a is the channel area.

A wide range of values have been reported in the literature for τ_{ep}. Dean and Pepper[26] have reported on a Si accumulation layer MOSFET. Extrapolating their results to 4.2 K we get $\tau_{\text{ep}}=4.8\times10^{-11}$ s. From measurements on an inversion layer MOSFET Neppl, Kotthaus, and Koch[11] obtain a scattering time of $\tau_{\text{ep}}=3.6\times10^{-9}$ s at 4.2 K. Our measurements of the I-V characteristic of sample 1 at 2.0 K allow us to set an upper bound on τ_{ep}.[13]

The power dissipated in the channel by I^2R heating will result in a parabolic term in the I-V curve. From the measured temperature coefficient of the conductance of 35 nA/K and the linearity of the I-V characteristic we deduce that an upper bound for τ_{ep} at 4.2 K is $\tau_{ep} \leq 4\times10^{-10}$ s. Finally using this value of τ_{ep} we deduce that the thermal impedance from the 2DEG to the lattice at 4.2 K is $R_{ep} \leq 1.5\times10^5$ K/W. This is not a surprising result considering the small volume (1×10^{-9} cm^3) of the channel within which the power is transferred from electrons to the phonons.

The bolometric sensitivity of the channel spins is given by the product of R_{ep} and the experimentally measured 35 nA/K temperature coefficient of the current. The 16 pW of power absorbed on resonance by the channel impurity electrons would then result in a bolometrically detected channel ESR signal of 80±40 fA. This upper bound is about three orders of magnitude *less* than the observed high power current signal in Fig. 5(a). Our estimate is conservative in view of the fact that we have not accounted for the T^{-n} dependence of the thermal impedance, which would result in a decrease in R_{ep} as the 2DEG heat up. Therefore, it is impossible to attribute the high power current signal (≥ -8 dBm) to bolometric detection of the channel ESR.

An additional experimental observation gives further weight to our conclusion. In sample 2 the high power current signal, attributed to SDT, was found to be positive from -10 to 19 dBm. However, from Fig. 6 the bolometric response, $d(I-I^0)/dP_\mu$ has changed sign over this power range. Mechanism 2 is simply not compatible with our experimental observations. In light of the fact that previous indirect ESR measurements of a 2DEG (Ref. 10) were attributed to bolometry or heating of the 2DEG, the above conclusion is a major result of this work.

In this section we have considered the possibility of bolometric detection of ESR in the sample. Although the low power current signal (≤ -20 dBm) was indeed shown to be due to bolometric detection of the bulk phosphorus ESR, we unequivocally eliminate the possibility that the high power current spectra (≥ -8 dBm) are due to bolometric detection of either the bulk or channel ESR. The observed magnitude, sign, and line shape of the SDT spectrum are not consistent with the predictions of the bolometric models shown in Fig. 7.

V. CHARACTERIZATION OF THE SDT SIGNAL

Having demonstrated that the high power current signal is due to spin-dependent transport, we characterized the SDT signal as a function of temperature, microwave power, Fermi energy of the 2DEG, and the orientation of the magnetic field. These investigations were exploratory in nature and serve to identify the primary questions that need to be asked to study spin-spin scattering in semiconductors.

A. Temperature and microwave power

Measurements of the current spectra over several decades of power were performed at 2.3 and 4.6 K. The low power current signal, due to bolometric detection of the bulk ESR, had the same line shape at both temperature. This is the anticipated result for an unsaturated ESR line. Accounting for the directly measured difference in bolometric sensitivity, the ratio of the areas of the absorption spectra at 2.3 and 4.6 K was $\sim 2.0x$. The susceptibility of the impurity electrons is expected to have a Curie law or T^{-1} temperature dependence, which is what we observe.

The high power current signal attributed to SDT has two features, a pair of hyperfine lines and a broad central feature. Figure 8 shows a plot of the peak amplitude of the integrated spectrum as a function of power at 2.3 and 4.6 K. The ratio of the 2.3 to 4.6 K data for the central features varies from $1.3x-1.5x$ and for the hyperfine feature from $1.4x-1.7x$. The line shape at $+7$ dBm or 5 mW is identical for both temperatures and narrows in a similar fashion with decreasing power.

From the expression for $\Delta I/I_0$ derived in the Sec. III A equation (13), there are two temperature-dependent terms, the impurity electron polarization (P_i^0) and the saturation parameter (s). We consider first the effect of the impurity electron polarization. P_i^0 is proportional to T^{-1} so both the hyperfine feature and the central peak, to the extent it is dominated by the impurity spins, should vary inversely with temperature. The reduction from the expected factor of 2 could indicate that the electron gas temperature (T_e) at 2.3 K is higher than the measured lattice temperature (T_l). The thermal impedance at 2.3 K obtained from Dean and Pepper's[26] measurements of the acoustic phonon scattering rate is 2×10^5 K/W.[13] The I^2R Joule heating for sample 1 biased under the conditions of Fig. 8, a drain-source voltage of 0.33 V and $I_0=10.0\ \mu$A, then gives a temperature rise of ~ 0.7 K.[13] If T_e is 3.0 K the ratio of the signals at the two temperatures is $1.5x$, which is within the range of the measured values.

The microwave power dependence of the current signal was measured over about five decades of power from 0.2

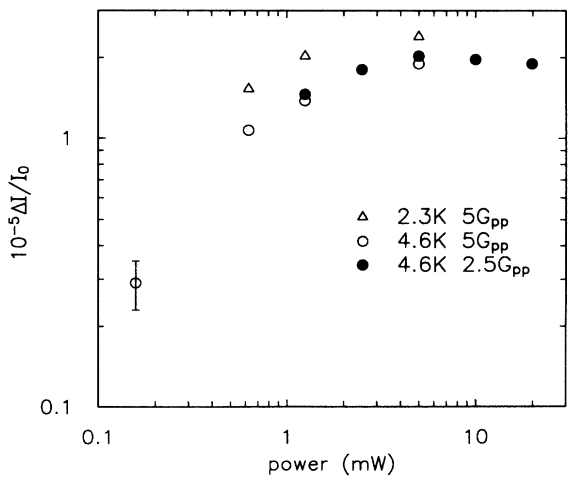

FIG. 8. Peak amplitude of the central feature from the integrated spectrum of sample 1; $n_s=0.57\times10^{12}$ cm^{-2} and $I_0=10.0\ \mu$A.

μW to 10 mW. The magnitude of the central feature from the high power SDT spectra (≥ -8 dBm) was shown in Fig. 8. Note that a complete study of the saturation behavior of the SDT signal is not possible because of interference from the bulk bolometric signal below -10 dBm. The expression for $\Delta I/I_0$ [Eq. (13)] indicates that at high power levels, as $s \rightarrow 1$, the SDT signal should become a constant independent of power. Above about 3 mW both the central and hyperfine features are approximately constant over the entire range of gate biases. This behavior would seem to confirm our predictions.

Before drawing any conclusions, however, we should consider the variation in line shape with power. The experimental data in Fig. 9 show that the line broadens with increasing power and the relative strength of the hyperfine feature with respect to the central component also grows. Assuming a homogeneously broadened line where the conduction and impurity spins saturate together, we have calculated the line shape at various microwave power levels.[13] We find that if the SDT spectra were indeed saturated, the ratio of the hyperfine to central components would grow much faster than in Fig. 9, i.e., the line would broaden much more significantly with increasing power. The magnitude of the SDT line indicates that the signal is fully saturated while the line shape is consistent with only a small degree of saturation. We believe that at high microwave power the sample is being heated by microwave dissipation in the stripline. Since $P_i^0 \sim T^{-1}$ the leveling off of the signal could be due to the decreasing impurity electron polarization. In addition, the heating of the 2DEG would also shorten the spin-lattice relaxation time T_1, which for an unsaturated line decreases s_i and s_c, thereby reducing the signal.

The experimental data on the power dependence of both the line shape and magnitude of the SDT signal cannot be satisfactorily explained without appealing to heating effects of one sort or another. The difficulty lies in separating the effects of sample heating from those due to the spin saturation parameter. Both I^2R Joule heating and microwave heating by the stripline need to be considered. To sort out these various effects we propose the following experiment. Fabricate a new sample on a wafer doped with $\sim 1\times 10^{16}$ P/cm^3. Since at this density the conventional ESR spectra consists of only two hyperfine split lines,[23] we eliminate the contribution of donor clusters from the central feature. Decreasing the donor density will also diminish the contribution to the central line from impurity spins that are strongly coupled to the conduction spins via T_{ix} processes. If the conduction and impurity spins are weakly coupled we expect to be able to separately observe the SDT signal from each spin species. In addition, to deduce the effect of microwave heating on T_e we may correlate measurements of the I-V characteristic of the MOSFET as a function of temperature, in the absence of microwave power, with measurements of the device I-V characteristic as a function of microwave power. Critical to clarification of the heating and saturation issues is working at lower donor concentrations and establishing a method to monitor the 2DEG temperature.

B. Fermi energy

One of the free parameters in this experiment is the Fermi energy or density of the 2DEG. The SDT signal was measured at 10 dBm over the range 0.10×10^{12} cm$^{-2} \leq n_s \leq 2.2\times 10^{12}$ cm^{-2}. As the density is increased by a factor of about 20 the central component of the line decreases by about two orders of magnitude (see Fig. 10); similar results were obtained for the hyperfine feature. From the conduction electron polarization term (P_c^0) in Eq. (8), we expect the SDT signal to scale as $(n_s)^{-1}$ or inversely with E_f, explaining a major portion of the density dependence. The singlet (Σ_s) and triplet (Σ_t) scattering cross sections, the 2DEG wave function, and the confining potential are all functions of E_f, so an n_s dependence is also expected from the parameter α in (9). Density dependence of the conduction spin-relaxation

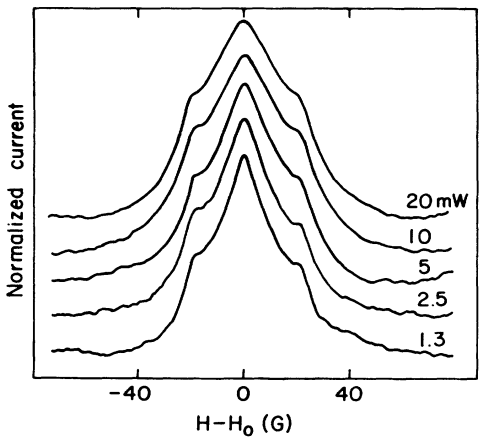

FIG. 9. Line-shape function for sample 1 at various power levels; $n_s = 0.57\times 10^{12}$ cm^{-2}, $I_0 = 10.0$ μA, $4.7 \leq T \leq 4.9$ K, and $H_{\rm mod} = 2.5$ G$_{pp}$.

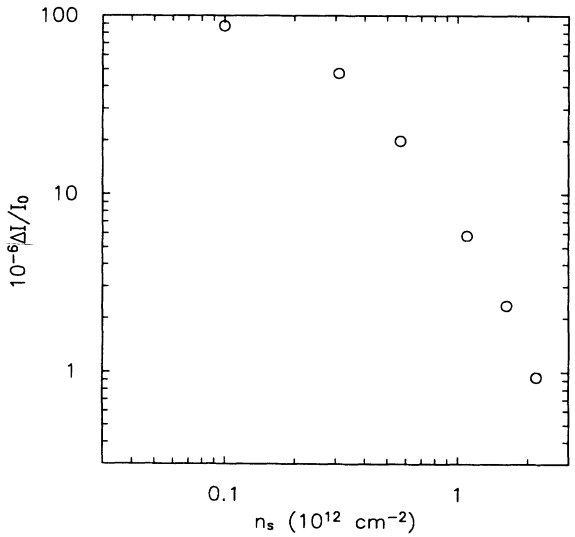

FIG. 10. Peak SDT signal as a function of density for sample 1; power = 10 dBm, $4.8 \leq T \leq 5.3$ K, and $H_{\rm mod} = 2.5$ G$_{pp}$.

TABLE I. Lower bound for $\langle \Sigma_s - \Sigma_t \rangle$ the difference in singlet and triplet scattering cross section integrated over θ and z, as a function of Fermi energy.

E_f (meV)	$n_s(10^{12}\ \mathrm{cm}^{-2})$	$\langle \Sigma_s - \Sigma_t \rangle (10^{-13}\ \mathrm{cm}^2)$
0.63	0.10	7
1.9	0.31	7
3.6	0.57	4
6.9	1.10	1.6
10.3	1.6	0.8
14	2.2	0.4

rate is another potential contributor to the n_s dependence of the signal magnitude.

From the data in Fig. 10 we calculate a lower bound for the integrated difference in singlet and triplet scattering cross section $\langle \Sigma_s - \Sigma_t \rangle$. The results obtained using the procedure described in Sec. IV A are listed in Table I. As discussed below, quantitative comparison of our experimental results with the formalism developed in Sec. IV A awaits calculation of the appropriate 2D scattering cross sections.

The variations of the line shape with density are shown in Fig. 11. The central peak narrows with increasing E_f and above a density of $1.1\times10^{12}\ \mathrm{cm}^{-2}$ the hyperfine feature drops off rather rapidly. The narrowing of the central feature could indicate an increase in the relative contribution of the conduction spins, over that of the impurity spins, to the SDT signal. In addition the coupling between the two spin systems via T_{ix}/T_{cx} processes is changing with density. Unfortunately, we cannot separate these two contributions in our experiment because both the conduction electrons and impurity spins contribute to the central feature. In a sample with a lower donor concentration and with appropriate relaxation times, we expect to be able to measure separately the impurity and conduction electron SDT signal.

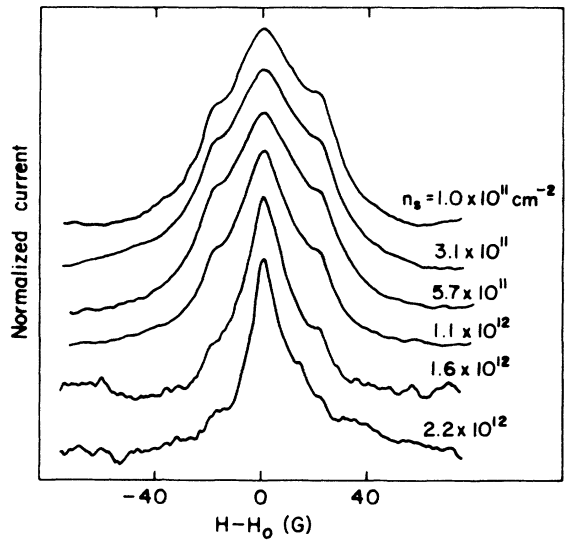

FIG. 11. SDT signal line shape for sample 1 at different densities; same conditions as Fig. 10.

The investigation of the Fermi energy dependence of the SDT signal was motivated by the known fact that in 3D the sign of α changes with energy.[22] For our 2D system $\Delta I/I_0 > 0$ in range of densities studied. The positive sign of the SDT signal clearly illustrates the inadequacy of using the 3D cross section for this problem. In three dimensions as the wave vector $k \to 0$, $\Sigma_s > \Sigma_t$ (Ref. 22) so Eq. (8) indicates that $\Delta I/I_0$ should be negative for low energy. Our data show that the SDT signal is positive and increasing as $k \to 0$. Therefore only a true 2D calculation of the scattering cross sections can adequately describe the SDT problem. We hope that the observed Fermi energy dependence of the signal together with the results in Table I will motivate such a calculation.

C. Magnetic-field orientation

For a spin-resonance experiment the ac magnetic field H_1 needs to be perpendicular to the dc magnetic field. In our experiment H_1 is oriented in the x direction (see Fig. 2), and H_{DC} was rotated in the y-z plane from perpendicular ($\mathbf{H}_0 = H_0\mathbf{z}$) to parallel ($\mathbf{H}_0 = H_0\mathbf{y}$) to the 2DEG interface. Only small changes in the magnitude of the SDT signal ($\sim$20%) were observed and the line shape was approximately the same.

In this work we are in the low-field regime with unresolved Landau levels so orientation effects due to Landau-level splitting are not expected. However, if the central feature has a significant contribution from the conduction electron spins, a g shift should be observed upon rotating the field. For the range of 2DEG density in this experiment, the conduction electrons occupy the lowest subband of the (100) surface[17] which corresponds to the two valleys oriented perpendicular to the interface. Wilson and Feher[27] have determined that the difference in g values with $\mathbf{H}_0$ parallel ($g_\parallel$) and perpendicular ($g_\perp$) to valley axis for Si:P is $g_\parallel - g_\perp = (1.04 \pm 0.04) \times 10^{-3}$. Using our resonant frequency of $\sim$8.9 GHz these values indicate that the central feature when the magnetic field is in the z direction should be about 1.7 G lower than when the field is in the y direction. The zero crossing of the central feature was carefully measured and a difference of (0.06±0.02) G was observed with the lower field value corresponding to $\mathbf{H}_0 = H_0\mathbf{z}$. We consider this to be essentially a null result. ESR experiments of Si inversion layer samples[28] have also failed to observe the g anisotropy, which is probably connected to the presence of strong disorder in his samples. In this study, if the central feature is dominated by exchange-coupled donors, we would not expect to see the conduction spin g anisotropy. The search for the expected g anisotropy is an additional reason for repeating the SDT experiment in a sample doped with $\sim 1\times10^{16}$ P/cm^3.

VI. CONCLUSIONS

A. Summary

The scattering of electrons by neutral impurities was proposed over 40 years ago by Pearson and Bardeen (1949). We have developed a new indirect spin-resonance

technique, spin-dependent transport (SDT), to demonstrate the scattering of a two-dimensional electron gas (2DEG) off neutral impurities in Si. SDT was observed by monitoring the conductivity of an accumulation layer transistor while modulating the electron-spin population. A microstrip resonator was incorporated into the structure to drive the electron-spin-resonance (ESR) transition.

Our technique utilizes the differences in singlet and triplet state cross sections for neutral impurity scattering to provide a sizable change in device current $\Delta I/I_0$ when the Zeeman resonance condition is satisfied. Based on a phenomenological model, $\Delta I/I_0$ was found in Eq. (13) to be proportional to the difference between the singlet and triplet scattering cross sections (via the parameter α), the equilibrium polarization of the conduction and impurity spin systems, and a saturation parameter, all weighted by the ratio of the relative strength of the neutral to total scattering rates. Modeling of the spin dynamics indicates that the SDT line shape is determined by the z dependence of the exchange interaction between the impurity and conduction spins, the direct coupling among the donor spins, and the spin-lattice relaxation rate.

The measured SDT spectrum consists of a broad central feature with the g value of conduction electrons in Si and a pair of narrow hyperfine peaks separated by 42 G. The central feature contains contributions from three sources: the conduction electron spins, exchange narrowed clusters of weakly coupled donor impurities, and impurity spins that are strongly coupled to the conduction spins via $1/T_{ix}$ processes. We assign the split pair to the impurity electron spin system. For a fixed gate bias and microwave power $\Delta I/I_0$ was a constant independent of I_0, as expected for a polarization-dependent change in conductivity. Alternative sources for the observed signal, such as microwave rectification in the contacts and bolometric detection of the electron-spin resonance, were explored and eliminated. The observed magnitude, line shape, and sign of the signal are incompatible with a bolometric model.

The data on temperature and microwave power dependence of the SDT spectra indicate that saturation and heating effects are both present in our sample. Future experiments on a sample with a lower donor density were proposed to sort out the influences of heating, clusters, and saturation on the SDT signal. Measurements were made with the magnetic field both parallel and perpendicular to the 2DEG interface, and only small changes in the SDT spectrum were observed. A possible g anisotropy from the conduction electron signal was not seen, but this is reasonable in view of the domination of the signal by the contribution from the impurity resonance. Again, an experiment at lower donor concentration would be very attractive.

A lower bound for difference between the singlet and triplet scattering cross sections integrated over θ and z, $\langle \Sigma_s - \Sigma_t \rangle$, was determined as a function of the Fermi energy of the 2DEG. $\langle \Sigma_s - \Sigma_t \rangle$ is greater than or equal to 4×10^{-13} cm^2 at a 2DEG of $n_s = 0.57\times10^{12}$ cm^{-2}. The positive sign of the SDT signal indicates that the interaction of a 2DEG with neutral impurities must be treated two dimensionally; scaling the known 3D scattering cross sections to their 2D counterparts is inappropriate. We hope our data on spin dependent transport in a 2DEG will motivate the calculation of the appropriate two-dimensional cross sections.

B. Spin resonance of confined structures

ESR is a powerful tool for studying the interaction of conduction electrons with local magnetic moments and the effects of a magnetic field on the motion of carriers in confined semiconductor systems. However, the small number of spins in two or lower dimensional devices precludes the utilization of conventional ESR methods. Using the spin-dependent transport technique in a micron size device, we expect to be sensitive to 10^4 or even fewer spins because the method exploits the effects of spin-dependent interactions on the sample conductivity instead of measuring directly the microwave power absorbed by the spin system. Thus SDT can be used as a sensitive probe of spin resonance in confined structures. For example, the typical sheet density for a Si MOSFET is $\sim10^{12}$ so that a 1×1 $(\mu m)^2$ device would contain only 10^4 spins, while GaAs heterostructures have an order of magnitude smaller sheet densities. Conventional ESR spectrometer sensitivity is about 10^{10} spins per gauss,[30] and Wallace[28] has recently reported on a microstrip induction spectrometer with a 10^8 spins per gauss sensitivity. For Si:P the hyperfine line is ~5 G wide, which puts a lower bound of 5×10^8 on the number of spins detectable by conventional ESR techniques. The linewidths for GaAs/AlAs quantum wells are about an order of magnitude wider, resulting in an even lower sensitivity in this system.

Our present device with a 1000×100 $(\mu m)^2$ gate contains 10^8–10^9 conduction electrons depending on the gate bias and $\sim10^8$ impurity electrons within the penetration depth of the 2DEG, a number which would be undetectable using conventional ESR techniques. To estimate the spin sensitivity obtainable via the SDT technique, we note that the measured derivative signal dI/dH is proportional to the current off-resonance I_0, but independent of the area of the device [see Eq. (13)]. For a MOSFET in which short channel effects are not important, the transistor current scales with the width to length ratio W/L. We expect to be able to reduce the device area by a factor of 10^4 and easily detect the SDT signal from 10^4 spins using our present experimental setup. Improvements in our measurement electronics would further enhance our spin sensitivity. Spin-dependent transport is an attractive technique for detecting spin-resonance effects in device size structures.

ACKNOWLEDGMENTS

We gratefully acknowledge the primary support of this work by the Office of Naval Research, Contract No. N0001491-J-1479 and the National Science Foundation, Contract No. DMR-8818558, through the Cornell Materials Science Center. The availability of the National Fabrication Facility and the support of its enthusiastic

staff were essential to the successful execution of this project. We would like to thank Tsuneya Ando for providing us with the calculations of the 2DEG density and self-consistent potential shown in Fig. 3.

APPENDIX

Simulations of line shapes, using the model for the spin dynamics discussed briefly in Sec. III B and given in more detail in the first half of the Appendix, have provided useful insights. Unfortunately, the complexities associated with the effects of direct exchange among donor spins within clusters[23,24] preclude a detailed comparison of the simulations with the observed line shape. Remember that the exchange coupling between the conduction and impurity spins $1/T_{ix}$ plays two roles in this theory: it is critical in the spin dynamics by transferring the saturation of weakly coupled spins to the conduction spins, and it is intimately related to the difference in singlet and triplet cross sections, the key ingredient of the SDT technique. In the second half of the Appendix we develop the relationship between these two roles in more detail.

1. Simulation

Three z coordinate values are introduced to define the locations of the three groups of impurity spins discussed in Sec. III B. The strongly coupled impurities lie between the limits z_1, defined as the minimum z at which the impurities are neutral rather than doubly occupied, and z_2, the depth at which the exchange scattering rate $1/T_{ix}(z)$ of the impurities against the conduction electrons is equal to one half the hyperfine splitting $A/2(=\frac{1}{2}\times 42=21$ G or 3.7×10^8 s^{-1}). The weakly coupled impurities lie between z_2 and z_3, being the depth below which the exchange rate for impurities is too small to influence the degree of saturation of the conduction spins. The defining condition for z_3 is that the exchange scattering rate $1/T_{ix}(z_3)$ is equal to $1/T_{i0}$, the bottlenecked rate of relaxation of the coupled spin system to the lattice,

$$\frac{1}{T_{ix}(z_3)}=\frac{1}{T_{i0}}=\left[\frac{\chi_c}{\chi_c+(z_3-z_1)\chi_i}\right]\frac{1}{T_{c1}} . \tag{A1}$$

χ_i and χ_c are, respectively, the impurity volume susceptibility and the conduction spin areal susceptibility, and $1/T_{c1}$ is the spin-lattice relaxation time for the conduction electrons. Finally, impurities below z_3 are the uncoupled impurities.

We write one Bloch equation for the conduction electrons and a set of $2r$ equations, indexed by $p=1,\ldots,r$, for slab number and $+$ or $-$ for the nuclear-spin orientation, for the impurities. The linearized Bloch equations take the form

$$\begin{aligned} i\omega M_c &= i\omega_0 M_c - M_c/T_2 \\ &\quad + \sum_{p=1}^{r} 1/T_{px}[(M_{p+}+M_{p-}) \\ &\qquad - M_c\chi_p/\chi_c] + i\gamma H_1\chi_c H_0 \cdots , \end{aligned}$$

$$\begin{aligned} i\omega M_{p+} &= i(\omega_0+1)M_{p+} - M_{p+}/T_2 \\ &\quad + 1/T_{px}[M_c\chi_p/2\chi_c - M_{p+}] + i\gamma H_1\chi_p H_0 , \end{aligned} \tag{A2}$$

$$\begin{aligned} i\omega M_{p-} &= i(\omega_0-1)M_{p-} - M_{p-}/T_2 \\ &\quad + 1/T_{px}[M_c\chi_p/2\chi_c - M_{p-}] + i\gamma H_1\chi_p H_0 \cdots . \end{aligned}$$

The M's are the amplitudes of the transverse magnetizations of the conduction spins (subscript c) and the impurities (indexed by slab number p and nuclear spin $+$ or $-$). ω_0 is the resonance frequency of the conduction spins and impurities (taken to be equal) in the static field H_0, ω the frequency of the microwave field, H_1 the magnitude of the rotating component of the microwave field, and γ the gyromagnetic ratio for the spins.

The $1/T_{px}\equiv 1/T_{ix}(z=z_p)$ are the exchange scattering rates for the impurities in the pth slab. Figure 3 indicates that all of the neutral impurities lie within the tail of the conduction electron wave function. We expect the exchange rate to fall rapidly moving from z_1 to z_3, reflecting a combination of the decrease in charge density with z as indicated in Fig. 3 and the decreasing overlap of the scattering potential into the accumulation channel with increasing depth of the impurity. For convenience in the simulation $1/T_{px}$ is assumed to depend exponentially on z, with a characteristic length z^*. $(1/T_{px})_{\max}$ is defined as the value of $1/T_{px}$ at $z=z_1$, and at $z=z_3$ $1/T_{px}$ is taken to be equal to $1/T_{i0}$. Among the parameters entering the simulation we have the greatest freedom in choosing the upper and lower limits on the exchange rates, $(1/T_{px})_{\max}$ and $1/T_{i0}$. The transverse relaxation times are, for convenience, taken to be the same for the conduction electrons and the impurities, $1/T_{c2}=1/T_{i2}\equiv 1/T_2$, with a value chosen to match the widths of the hyperfine features in the observed spectra.

The partial susceptibilities of the slabs χ_p and the conduction spin susceptibility χ_c have units of length since they describe a magnetic moment per unit area and not volume. The χ_p are given in terms of the bulk (volume) impurity susceptibility χ_i by $\chi_p=\chi_i\times$ (thickness of pth slab). The susceptibility ratio for a donor density of 3×10^{17} cm^{-3} and a temperature of 4 K is $\chi_c/\chi_i=2\times 10^{-7}$ cm. The simulations were run for an assumed value of $z_3-z_1=10^{-6}$ cm.

The equations, in steady state, may then be solved by computer and the partial magnetizations summed to give the total transverse magnetization which in turn is proportional to the power absorbed from the microwave field. Under the approximation of weak saturation parameter s_c is proportional to the absorbed power and hence to the total transverse magnetization. We calculate only normalized line shapes, not magnitudes, since we have no very reliable knowledge of the spin-lattice time for the conduction electrons.

The simulation, as anticipated, gives the hyperfine split wings and the central component containing contributions from both the conduction electrons and the exchange narrowed resonance of the strongly coupled impurities. Reasonable fits to the experimental data are

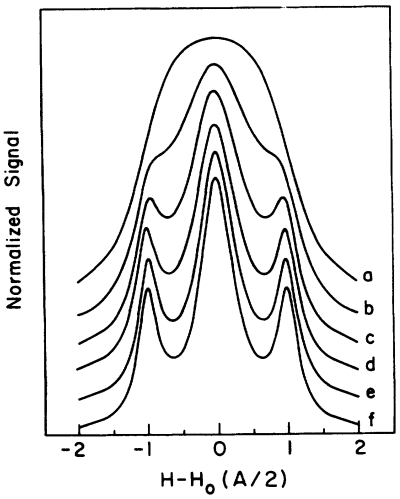

FIG. 12. Simulated line shapes for the case of equal numbers of strongly and weakly coupled impurity spins and a fixed susceptibility ratio $\chi_c/[\chi_i(z_3-z_1)]=0.2$. The ratios of maximum to minimum exchange rate $(1/T_{ix})_{\max}/(1/T_{i0})$ vary from 10 to 10^6 in steps of $\times 10$ for curves $a-e$.

possible. Though the specific fitting parameters are not of great significance because of the neglect of the direct impurity-impurity exchange, the fits are of interest in setting bounds on some of the parameters and in revealing the relevant physics. The accompanying figures illustrate a few of the results.

Figures 12 and 13 give simulations for a variety of exchange rates. In Fig. 12 the geometric mean of the maximum and minimum rates is kept fixed and equal to the half-hyperfine splitting. This condition corresponds to equal numbers of weakly and strongly coupled impurities. The range of rates, from $1/T_{i0}$ to $(1/T_{px})_{\max}$, is varied

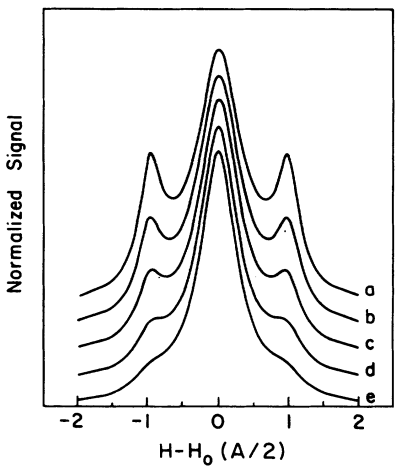

FIG. 13. Simulated line shapes for the case of a fixed ratio of maximum to minimum exchange rates $(1/T_{ix})_{\max}/(1/T_{i0})=10^4$ and a fixed susceptibility ratio $\chi_c/[\chi_i(z_3-z_1)]=0.2$. The geometric mean of the rates $[(1/T_{ix})_{\max}(1/T_{i0})]^{1/2}$ varies from 1 to 10 in steps of $10^{1/4}$ for curves $a-e$. The corresponding range of the ratio of numbers of weakly to strongly coupled spins is 1/1 to 1/3.

from 10 to 10^6. For curve a, the minimum exchange range for the ions is still fast enough to exchange broaden even the most weakly coupled of the coupled impurities, and no hyperfine structure can be resolved. Also, the most strongly coupled of the impurities still are not exchanging rapidly enough to narrow the hyperfine splitting very dramatically. The resulting line is broad and without structure. As the ratio of maximum to minimum rates is increased to 10^2 in curve b, there begin to be enough impurity spins with adequately slow exchange rates to give a hint of the hyperfine components. With increasing range of exchange rates, the hyperfine components develop increasing strength as a greater fraction of the spins are weakly enough coupled to contribute fully to the hyperfine components. At the same time, the strongly coupled spins are, for the most part, heavily narrowed and contribute strongly to the central line.

Figure 13 gives a different cut, in which the range of exchange rates, $(1/T_{px})_{\max}/(1/T_{i0})$, is left at 10^4 but the geometric mean is varied from the half-hyperfine rate to a value ten times the half-hyperfine rate. This is equivalent to a variation of the ratio of weakly coupled to strongly coupled impurities. For curve a, 50% of the impurities are weakly coupled, 50% strongly coupled. The range of exchange rates is adequate that a substantial fraction of weakly coupled impurities are not broadened by the exchange and most of the strongly coupled ones are in the strongly narrowed limit. As the mean rate is increased, keeping the range of rates fixed, we see the transfer of intensity from the hyperfine to the central components as well as a narrowing of the central component as the strongly coupled spins are carried further into the strongly narrowed limit. In curve e the hyperfine lines have become quite weak, in part because of the smaller number, 25%, of weakly coupled spins, but more importantly, because of these, only a small fraction are weakly enough coupled to avoid the exchange broadening which carries their contributions into the broad tails of the central line.

For both of these figures, the relative susceptibility $\chi_c/[\chi_i(z_3-z_i)]$ was taken to be 0.2. Thus in these figures the central part is dominated by the exchange-narrowed impurity resonance, the conduction spins making a relatively minor contribution. The model can also explore the consequences of reducing the impurity concentration as illustrated in Fig. 14. As expected, the relative contribution in the hyperfine wings decreases with decreasing impurity susceptibility. The conduction spins in curve e, for which the relative susceptibility is 20, now dominate the central component rather than the exchange-narrowed impurity spins. The linewidth in e is determined principally by $1/T_2$, in contrast with e of Fig. 13 in which the width is dominated by the incomplete narrowing of the hyperfine splitting.

2. Signal strength

As noted earlier, the exchange rates which influence the spin dynamics are intimately connected with the difference in singlet and triplet cross sections which determine the magnitude of the SDT signal through Eqs. (9) and (13). In this section we develop very rough quan-

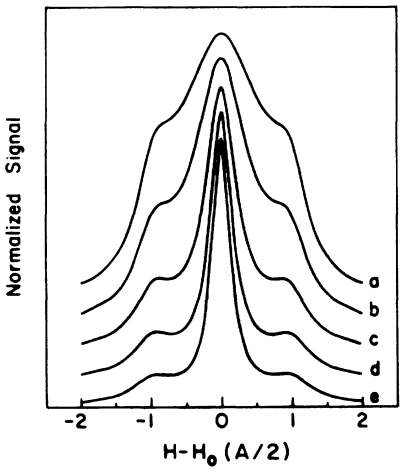

FIG. 14. Simulated line shapes for a fixed ratio of the numbers of weakly and strongly coupled impurity spins equal to unity, and a fixed ratio of maximum to minimum exchange rate $(1/T_{ix})_{\max}/(1/T_{i0})=10^2$. The susceptibility ratio $\chi_c/[\chi_i(z_3-z_1)]$ varies from 0.2 in curve *a* to 20 in curve *e* in steps of $10^{1/2}$.

titative arguments to predict the SDT signal magnitude from features of the experimental signal line shape. The simulations described in the preceding section have provided essential insight for this analysis; they have not provided a more direct route because of the difficulty of including effects of the direct donor-donor exchange.

If the differential scattering amplitudes for "direct" and "exchange" scattering[7] are denoted $f(\theta;z)$ and $g(\theta;z)$, the differential singlet (triplet) scattering cross sections at depth z are given by $\Sigma_{s(t)}(z)=[f(z)+(-)g(z)]^2$. The difference in cross section for impurities at depth z is then given in terms of f and g by $\Sigma_s(z)-\Sigma_t(z)=4f(z)g(z)$. In a similar fashion the spin-flip cross section is given by $\Sigma_{sf}(z)=g(z)^2$.

A connection between the transport cross sections and the parameters of the spin dynamics model is established as follows. First we express the total conduction exchange scattering rate in terms of the ion exchange rate entering the spin dynamics equations by

$$\frac{1}{T_{cx}}=\frac{\chi_i}{\chi_c}\int_{z_1}^{z_3}\frac{1}{T_{ix}}(z)dz$$
$$=\frac{\chi_i}{\chi_c}\left[\frac{1}{T_{ix}}\right]_{\max}(z_3-z_1)\left[\ln\frac{\left[\frac{1}{T_{ix}}\right]_{\max}}{\left[\frac{1}{T_{i0}}\right]}\right]^{-1}$$
$$\equiv\frac{\chi_i}{\chi_c}\left[\frac{1}{T_{ix}}\right]_{\max}z^*\,, \tag{A3}$$

where the assumed exponential dependence of $1/T_{ix}$ on z is characterized by the length z^* and we have taken $1/T_{ix}(z_3)\ll 1/T_{ix}(z_1)$. In terms of the spin-flip cross section $\Sigma_{sf}(z)$ we have

$$\frac{1}{T_{cx}}=N_D v\int_{z_1}^{z_3}dz\int d\theta\,\Sigma_{sf}(\theta;z)$$
$$=N_D v\int_{z_1}^{z_3}dz\int d\theta\,g(\theta;z)^2\,. \tag{A4}$$

In Eq. (9) the numerator of α is given by an integral of the difference in singlet and triplet cross sections. Equating the two expressions above for $1/T_{cx}$ we may evaluate α of Eq. (9) as

$$\alpha=\langle\Sigma_s+3\Sigma_t\rangle^{-1}\int d\theta(1-\cos\theta)\int dz(\Sigma_s-\Sigma_t)$$
$$=\langle\Sigma_s+3\Sigma_t\rangle^{-1}\int d\theta(1-\cos\theta)\int dz\,4fg$$
$$=\frac{4z^*}{N_D v\langle\Sigma_s+3\Sigma_t\rangle}\frac{\int d\theta(1-\cos\theta)\int dz\,fg}{\int d\theta\int dz\,g^2}\frac{\chi_i}{\chi_c}\left[\frac{1}{T_{ix}}\right]_{\max}. \tag{A5}$$

Noting the definition of $1/\tau_{n0}$ in Eq. (9) and using Eq. (A5) allows Eq. (13) to be written

$$\frac{\Delta I}{I}\cong -P_i^0P_c^0\,s\frac{(N_D v/4)\langle\Sigma_s+3\Sigma_t\rangle}{1/\tau_t}\alpha$$
$$=-P_i^0P_c^0\,s\,\frac{(1/T_{ix})_{\max}}{1/\tau_t}\frac{\chi_i z^*}{\chi_c}\frac{\int d\theta(1-\cos\theta)\int dz\,fg}{\int d\theta\int dz\,g^2} \tag{A6}$$

To proceed further we replace the ratio of integrated scattering factors by unity, consistent with the typical value of $f/g\sim 1$ for the three-dimensional scattering cross sections in Ref. 22. For comparison with experiment we note that saturation parameter $s\le 1$ and therefore replace the equality in Eq. (A6) by the inequality

$$\frac{\Delta I}{I}\le -P_i^0P_c^0\frac{(1/T_{ix})_{\max}}{1/\tau_t}\frac{\chi_i z^*}{\chi_c}\,. \tag{A7}$$

This gives an expression relating the observed signal strength to a relaxation rate which may be estimated, albeit only very roughly, from the line-shape results.

We work with the data set taken at an electron concentration of $n_s=0.57\times 10^{12}$ cm^{-2} to see whether there is

plausible consistency in this comparison. The survival of resolvable intensity in the hyperfine components of the SDT spectrum, despite the combined effects of the exchange due to clustering[23,24] and the exchange with the conduction electrons, gives an estimate of the relative numbers of weakly and strongly coupled spins. This number is obtained from comparisons of the intensities of the hyperfine components relative to the central line in the SDT and ESR line shapes [e.g., (a) and (d) of Fig. 5], together with an assumed value for the depth of interacting impurities z_3-z_1. For the moment we assume $z_3-z_1=400$ Å. Comparison of Figs. 5(a) and 5(d) then gives a ratio of the number of weak to the number of strong impurities of $(w/s)=2.0\pm0.6$. We explore later the consequences of alternative choices of z_3-z_1.

Elliot's[30] result relating the conduction spin-relaxation rate to the total impurity scattering rate, which we know from the sample mobility, gives $0.003\leq 1/T_{c1}\leq 0.03$ (in units of $A/2$ or 4×10^6 s^{-1}), where we have arbitrarily assigned an uncertainty range of an order of magnitude. Equation (A1) then yields $1.7\times10^{-4}\leq 1/T_{i0}\leq 1.5\times10^{-3}$. The assumption of an exponential dependence of the exchange rate upon depth allows estimation of the maximum exchange rate $1/T_{ix}|_{\max}$ from $1/T_{i0}$ and the ratio of numbers of weakly and strongly coupled impurities (w/s) using $w/s=-\ln(1/T_{i0})/\ln(1/T_{ix}|_{\max})$. Equation (A3) then gives, in addition, a value for z^*. The assumption of $z_3-z_1=400$ Å gives finally $10\leq T_{ix}|_{\max}\leq 400$, and $z^*=35\pm10$ Å. The scale length of the assumed exponential dependence of the exchange rate is moderately well defined by this procedure; the magnitudes of the exchange rates are given only very roughly.

Choosing other values of z_3-z_1 in the range 100–1000 Å and taking $1/T_{c1}=0.01$ gives z^* in the range 10–80 Å and $1/T_{ix}|_{\max}$ in the range 6–1000. Equation (A6) allows a comparison with experiment, with the predicted result $1\times10^{-7}\leq\Delta I/I\leq 1\times10^{-4}$. The experimental value of $\Delta I/I\cong 20\times10^{-6}$ is at one end of this range; the values $z_3-z_1\sim1000$ Å, $z^*\sim60$ Å, and $1/T_{ix}|_{\max}\sim200$ are then consistent with the magnitude of the observed signal. This consistency adds to our confidence in the interpretation of this experiment as the successful detection of an SDT signal.

*Present address: National Institute of Standards and Technology, Electricity Division, Gaithersburg, MD 20899.

[1]G. L. Pearson and J. Bardeen, Phys. Rev. **75**, 865 (1949).
[2]Cavid Erginsoy, Phys. Rev. **79**, 1013 (1950).
[3]B. K. Ridley, *Quantum Processes in Semiconductors,* 2nd ed. (Clarendon, Oxford, 1988), pp. 152–161.
[4]P. Norton, T. Braggins, and H. Levinstein, Phys. Rev. B **8**, 5632 (1973).
[5]R. Baron, M. H. Young, and T. C. McGill, in *Proceedings of 13th International Conference on the Physics of Semiconductors,* Rome 1976, edited by F. G. Fumi (North-Holland, New York, 1976), pp. 1158–1165.
[6]J. Schmidt and I. Solomon, C. R. Acad. Sér. B **263**, 169 (1966); Ionel Solomon, in *Proceedings of the XIth International Conference on the Physics of Semiconductors, Warsaw, Poland* (Elsevier, New York, 1972), pp. 1–37.
[7]A. Honig, Phys. Rev. Lett. **17**, 186 (1966).
[8]R. Maxwell and A. Honig, Phys. Rev. Lett. **17**, 188 (1966).
[9]D. D. Thorton and A. Honig, Phys. Rev. Lett. **30**, 909 (1973).
[10]D. Stein, K. v. Klitzing, and G. Weimann, Phys. Rev. Lett. **51**, 130 (1983).
[11]F. Neppl, J. P. Kotthaus, and J. F. Koch, Phys. Rev. B **19**, 5240 (1979).
[12]A brief summary of this work appears in Ruby N. Ghosh and Robert H. Silsbee, Solid State Commun. **81**, 545 (1992).
[13]Ruby N. Ghosh, Ph.D. thesis, Cornell University, 1991.
[14]Ruby N. Ghosh and Robert H. Silsbee, Cryogenics **30**, 1069 (1990).
[15]Tsuneya Ando, Phys. Rev. B **13**, 3468 (1976).
[16]Frank Stern, Phys. Rev. Lett. **33**, 960 (1974).
[17]Tsuneya Ando (private communication).
[18]Frank Stern and W. E. Howard, Phys. Rev. **163**, 816 (1967).
[19]S. Chandrasekhar, Astrophys. J. **100**, 176 (1944).
[20]Nunzio O. Lipari, J. Vac. Sci. Technol. **15**, 1412 (1978).
[21]P. Norton, J. Appl. Phys. **4**, 308 (1976).
[22]Philip G. Burke and Harry M. Schey, Phys. Rev. **126**, 163 (1972).
[23]D. New and T. G. Castner, Phys. Rev. B **29**, 2077 (1984).
[24]D. New, Phys. Rev. B **32**, 2419 (1985).
[25]G. Feher, Phys. Rev. **114**, 1219 (1959).
[26]C. C. Dean and M. Pepper, J. Phys. C **17**, 5663 (1984).
[27]D. K. Wilson and G. Feher, Phys. Rev. **124**, 1068 (1961).
[28]W. J. Wallace and R. H. Silsbee, Phys. Rev. B **44**, 12964 (1991).
[29]K. L. Brower, Appl. Phys. Lett. **43**, 1111 (1983).
[30]R. J. Elliott, Phys. Rev. **96**, 266 (1954).